IEEE Access
Multidisciplinary | Rapid Review | Open Access Journal

Received December 24, 2018, accepted January 6, 2019, date of publication January 15, 2019, date of current version February 6, 2019.

Digital Object Identifier 10.1109/ACCESS.2019.2892995

Wide-Band Filtering Three-Port Coupler With Inherent DC-Blocking Function

WEIMIN WANG[1], YANA ZHENG[1], YONGLE WU[1,2], (Senior Member, IEEE), ZHENG ZHUANG[1], AND YUANAN LIU[1]

[1]Beijing Key Laboratory of Work Safety Intelligent Monitoring, School of Electronic Engineering, Beijing University of Posts and Telecommunications, Beijing 100876, China

[2]State Key Laboratory of Information Photonics and Optical Communications, School of Electronic Engineering, Beijing University of Posts and Telecommunications, Beijing 100876, China

Corresponding author: Yongle Wu (wuyongle138@gmail.com)

This work was supported in part by the National Natural Science Foundation of China under Grant 61671084 and Grant 61821001, in part by the Guangzhou Major Projects of Industrial Technology of China (Research and Development of Large-scale Multi-beam Antenna Array for 5G Massive MIMO Communication) under Grant 201802010052, and in part by the Fund of State Key Laboratory of Information Photonics and Optical Communications, Beijing University of Posts and Telecommunications, China, under Grant IPOC2017ZR06.

ABSTRACT This paper presents a novel wide-band filtering three-port coupler with inherent DC-blocking function, which is simply comprised of a power divider with wideband filtering function and a broadband phase shifter with a modified coupled line. For demonstration, a designed prototype operating at 3 GHz is simulated, fabricated, and measured. From the simulated and measured results, the coupler shows a 49% filtering bandwidth with 12-dB return loss and $90° \pm 5°$ phase shifting. The amplitude imbalance between the two output ports is less than 0.5 dB. The all-passband isolation is below -13 dB and the 25.7-dB upper stopband rejection is up to 5.4 GHz. Good agreement between the simulated and measured results validates the proposed idea. Hence, the proposed coupler is well suited for the applications of wideband, filtering, and single-layer circuitry integration.

INDEX TERMS Coupler, power divider, phase shifter, wideband, filtering, DC-blocking.

I. INTRODUCTION

Hybrid couplers with 180° or 90° phase difference play an important role in the radio frequency (RF) field and the microwave field. It is widely used in microwaves and a variety of different wireless communication systems, especially for balanced power amplifiers, balanced mixers and various antenna feed networks. Specially, the 90° hybrid coupler is widely used in multi-feed circularly polarized (CP) antennas [1]–[3], Doherty amplifiers, image rejection mixers, etc. In recent years, as the key component of the RF front end, couplers and filters are in increasing demand of being low loss, widely tunable, compact structure, low cost, and convenient installation. In order to further suppress the interfering signal of the frequency/microwave front end, the coupler is usually connected in series with the filter, which results in a bulky circuit size and high insertion loss. Due to high frequency selectivity and miniaturization, microwave devices with filtering performance have been extensively studied [4]–[7].

To meet the requirement of wide-band communication systems with circularly polarized antennas, many efforts have been made to broaden the bandwidth of hybrid couplers [8]–[14]. Owing to the fact that the conventional branch-line directional coupler is only suitable for narrow-band systems [8], the multi-section branch-line topology and defected ground structure have been presented for enhancing bandwidths [9]–[11]. However, it is noted that the cascaded multi-section structure occupies large circuit area. In [12], an improved branching line coupler on a single-layer circuit board is proposed, but this coupler still has a complex circuit board structure. The broadside coupled microstrip/slot couplers can operate over ultra-wideband, but the three-layer structures may increase circuit complexity and cause incompatibility with other components during circuit integration [13], [14]. The single-layer edge-coupled microstrip couplers are simple in structure and low in cost, but the bandwidth is less than 25% [15], [16].

Some three-port couplers consisting of balanced power dividers and phase shifters also achieve significant characteristics of the hybrid circuits. A variety of RF devices can be implemented through a combination of different balanced power dividers [17]–[22] and phase shifters. In [23],

a wide-band planar balun includes a two-way Wilkinson power divider and a broad-band 180° phase shifter has been presented. In [24] and [25], the hybrid coupler consists of a wideband power divider and a wideband 90° phase shifter to achieve wideband performance. Nevertheless, they did not implement filtering performance and all-passband isolation that might lead to some interfering signals at the RF front end. To the best of authors' knowledge, there are few studies on broadband hybrid couplers with filtering performance and DC-blocking function in complex multi-function systems.

In this paper, a wide-band filtering three-port coupler with inherent DC-blocking function is proposed and developed. The coupler consists of a broadband power divider with filtering performance [26] and a wideband 90° phase shifter [27]. For the proposed hybrid coupler, the simulated and measured results show that the operational bandwidth (2.1-3.57 GHz) over 12-dB return loss is approximately 49%. Moreover, the upper stopband of the proposed coupler is extended up to 5.4 GHz with the suppression level above 25.7-dB and the all-passband isolation is below −13 dB. The proposed wideband filtering coupler has a wide bandwidth, high all-passband isolation, an excellent out-band rejection, and DC-blocking between two output ports. For verification, the microstrip prototype is simulated, fabricated, and measured. Good agreement between the simulated and the measured results validate the proposed design concept.

II. THEORETICAL ANALYSIS

Fig. 1 shows the circuit model of the proposed wide-band filtering three-port coupler, which is composed of a wide-band filtering power divider and a wide-band coupled-line phase shifter.

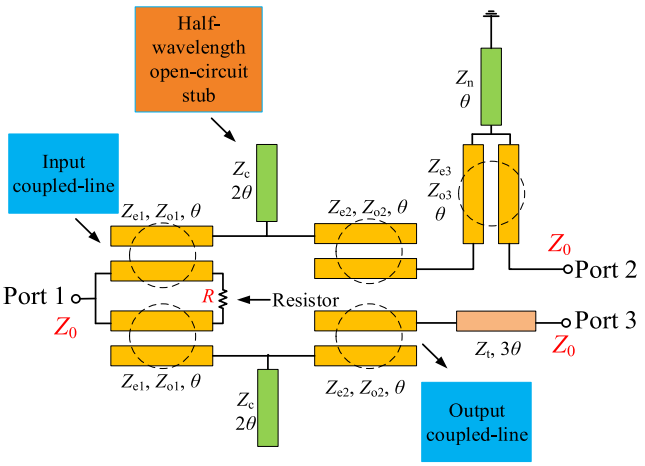

FIGURE 1. The circuit configuration of the proposed wide-band filtering three-port coupler.

A. FILTERING POWER DIVIDER

For the filtering power divider (FPD), it comprises cascaded coupled-line sections (CLs) with tight coupling and half-wavelength open-circuit stubs (OCSs). The designed OCS introduces extra transmission poles (TPs) and transmission zeros (TZs) at the cut-off frequency to obtain a wide stopband and enhance the high frequency selectivity. In addition, two cascaded CLs can extend the impedance transforming. Note that a single resistor is utilized to achieve the high all-passband isolation between input CLs. By using traditional even-/odd-mode analysis to simplify the circuit structure, we obtain the S-parameters of the FPD. The corresponding even-/odd-mode equivalent circuits are shown in Fig. 2. In the even-/odd-mode equivalent circuits, for simplification we have assumed that [26]

$$\begin{cases} Z_{a1} = \dfrac{Z_{e1} + Z_{o1}}{2} \\ Z_{b1} = \dfrac{Z_{e1} - Z_{o1}}{2}, \end{cases} \tag{1a}$$

$$\begin{cases} Z_{a2} = \dfrac{Z_{e2} + Z_{o2}}{2} \\ Z_{b2} = \dfrac{Z_{e2} - Z_{o2}}{2}, \end{cases} \tag{1b}$$

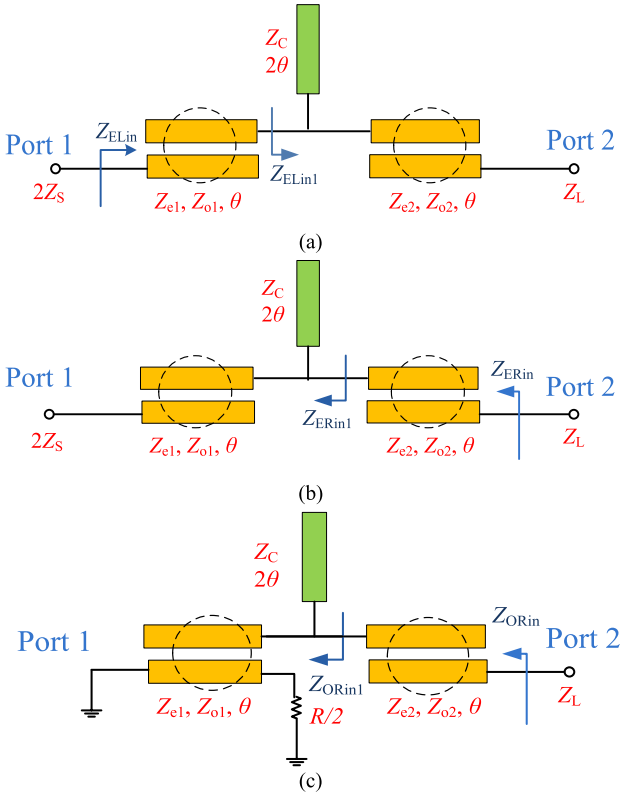

FIGURE 2. Equivalent circuits of the proposed FPD [26]. (a) Even mode with left-hand side excitation. (b) Even mode with right-hand side excitation. (c) Odd mode with right-hand side excitation.

where the subscript e and o denote the even- and odd-mode, respectively. Based on (1a) and (1b), the even-/odd-mode input impedances of the wideband filtering coupler with the left- and right-hand side excitation can be derived as:

$$Z_{ELin} = -jZ_{a1}\cot\theta + \frac{Z_{b1}^2 \csc^2\theta}{Z_{ELin1} - jZ_{a1}\cot\theta}, \tag{2}$$

$$Z_{\mathrm{ERin}} = -\mathrm{j}Z_{\mathrm{a2}}\cot\theta + \frac{Z_{\mathrm{b2}}^2\csc^2\theta}{Z_{\mathrm{ERin1}} - \mathrm{j}Z_{\mathrm{a2}}\cot\theta}, \tag{3}$$

$$Z_{\mathrm{ORin}} = -\mathrm{j}Z_{\mathrm{a2}}\cot\theta + \frac{Z_{\mathrm{b2}}^2\csc^2\theta}{Z_{\mathrm{ORin1}} - \mathrm{j}Z_{\mathrm{a2}}\cot\theta}, \tag{4}$$

where θ is the electrical length of CLs and Z_{ELin1}, Z_{ERin1}, and Z_{ORin1} can be obtained through [26]. Therefore, the reflection coefficient $\Gamma_{\mathrm{in}}{}^{\mathrm{e}}$ at the input port 1 and the corresponding reflection coefficient $\Gamma_{\mathrm{out}}{}^{\mathrm{e}}$ and $\Gamma_{\mathrm{out}}{}^{\mathrm{o}}$ at the output port 2 can be calculated as:

$$\Gamma_{\mathrm{in}}^{e} = \frac{Z_{\mathrm{ELin}} - 2Z_{\mathrm{S}}}{Z_{\mathrm{ELin}} + 2Z_{\mathrm{S}}}, \tag{5}$$

$$\Gamma_{\mathrm{out}}^{e} = \frac{Z_{\mathrm{ERin}} - Z_{\mathrm{L}}}{Z_{\mathrm{ERin}} + Z_{\mathrm{L}}}, \tag{6}$$

$$\Gamma_{\mathrm{out}}^{o} = \frac{Z_{\mathrm{ORin}} - Z_{\mathrm{L}}}{Z_{\mathrm{ORin}} + Z_{\mathrm{L}}}, \tag{7}$$

where Z_{S} is the source impedance and Z_{L} denotes the load impedance. Additionally, the values of Z_{S} and Z_{L} are 50 Ω. The S-parameters can be found through the reflection coefficients of the even- and odd-mode equivalent circuits.

$$S_{11} = \Gamma_{\mathrm{in}}^{\mathrm{e}}, \tag{8}$$

$$S_{23} = \frac{\Gamma_{\mathrm{out}}^{\mathrm{e}} - \Gamma_{\mathrm{out}}^{\mathrm{o}}}{2}. \tag{9}$$

Therefore, when the electrical length of CLs is $\theta = \pi/2$ at the center frequency $f_0 = 3$ GHz, it can satisfy the input matching S_{11} with broadband filtering performance and high isolation ($S_{23} = 0$). Then, based on (8) and (9), we can get the electrical lengths of the half-wavelength OCSs.

B. WIDE-BAND COUPLED-LINE PHASE SHIFTER

For the wide-band coupled-line phase shifter, we assume the parameter ρ in (10) is used to denote the coupling strength of the coupled line [27]. The circuit configuration of the phase shifter is shown in Fig. 3.

$$\rho = \frac{Z_{\mathrm{e3}}}{Z_{\mathrm{o3}}} (\rho \geq 1). \tag{10}$$

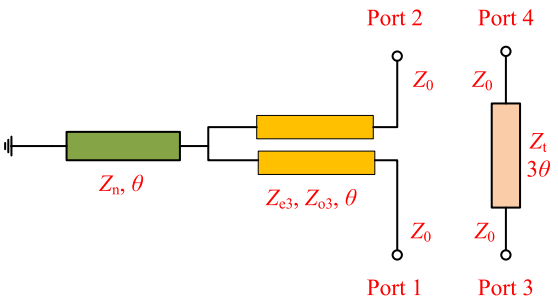

FIGURE 3. Circuit configuration of the proposed wide-band coupled-line phase shifter [27].

Then, the odd- and even-mode characteristic impedances Z_{e3} and Z_{o3} can be written as:

$$\begin{cases} Z_{\mathrm{e3}} = Z_{\mathrm{m}}\sqrt{\rho} \\ Z_{\mathrm{o3}} = Z_{\mathrm{m}}/\sqrt{\rho}, \end{cases} \tag{11}$$

where Z_{m} is the image impedance and the coupling coefficient of the coupled line can be expressed as:

$$C(\mathrm{dB}) = -20\lg\left(\frac{\rho - 1}{\rho + 1}\right). \tag{12}$$

Then, the phase difference is presented as:

$$\Delta\Phi = \mathrm{Phase}(S_{21}) - \mathrm{Phase}(S_{43}). \tag{13}$$

Moreover, the bandwidth of the phase deviation can be estimated by the slope (K) of phase difference at the center frequency $f_0 = 3$ GHz.

$$K = \left.\frac{\partial(\Delta\Phi)}{\partial\theta}\right|_{f=f_0} = 3 - \left(\frac{\sqrt{\rho}}{Z_{\mathrm{m}}} + Z_{\mathrm{m}}\sqrt{\rho} + \frac{Z_{\mathrm{m}}^2\rho}{2Z_{\mathrm{n}}}\right). \tag{14}$$

III. PARAMETER ANALYSIS

In this section, we discuss about the influence of R, Z_{c}, Z_{e3}, and Z_{o3} on the overall performances involving in-band return loss, all-passband isolation, stopband suppression, and phase difference. Furthermore, we will see the effect of the proposed coupler with/without OCSs on circuit bandwidth, phase deviation and filtering performance.

As depicted in Fig. 4, the proposed wideband filtering coupler with different free variables (R, Z_{c}, Z_{e3}, and Z_{o3}) is designed and simulated. The S-parameters as a function of the frequency for the proposed wideband filtering coupler with optimal impedances of $Z_{\mathrm{e1}} = 154$ Ω, $Z_{\mathrm{o1}} = 44$ Ω, $Z_{\mathrm{c}} = 28$ Ω, $Z_{\mathrm{e2}} = 160$ Ω, $Z_{\mathrm{o2}} = 70$ Ω, $Z_{\mathrm{t}} = 50$ Ω, $Z_{\mathrm{e3}} = 46$ Ω, $Z_{\mathrm{o3}} = 28$ Ω, $Z_{\mathrm{n}} = 42$ Ω, $Z_{\mathrm{S}} = Z_{\mathrm{L}} = 50$ Ω, and $\theta = \pi/2$. In order to obtain wideband and high isolation, R can be tuned and the optimal parameter of R can be obtained as shown in Fig. 4(a). From Fig. 4(a), when R increases from 50 to 197 Ω, the in-band return loss is improved. However, as the value of R increases to 500 Ω, the return loss of the proposed coupler is getting worse. In addition, the isolation becomes worse as R decreases from 197 to 50 Ω. Therefore, the value of R is optimized as 197 Ω for the desired in-band bandwidth and the all-passband isolation. Fig. 4(b) shows how the values of Z_{c} affect the performances of return loss and isolation with $R = 197$ Ω. Moreover, the analysis of Z_{c} is similar to R and the optimal Z_{c} should be found by the tuning process. It can also be seen that the value of Z_{c} changes from 10 to 28 Ω, the in-band bandwidth increases significantly despite the deterioration of the isolation. It's easy to find that the bandwidth increases when the value of Z_{c} continues to increase to 35 Ω, the in-band return loss is reduced. From the above, the optimal value of Z_{c} is 28 Ω. Based on the above analysis and conclusions we can obtain from Fig. 4(c) the effect of Z_{e3}, and Z_{o3} on the S-parameters and phase difference of the circuit as well. In Fig. 4(c), $Z_{\mathrm{e3}} = 30$ Ω and $Z_{\mathrm{o3}} = 20$ Ω perform widest bandwidth although the in-band return loss and ±5° phase variation are unsatisfactory. With Z_{e3} and Z_{o3} increase, the bandwidth and phase shift of the coupler are improved. It can be seen from Fig. 4(c) that when $Z_{\mathrm{e3}} = 46$ Ω, and $Z_{\mathrm{o3}} = 28$ Ω, the coupler's bandwidth and phase shift characteristics achieve the best performance.

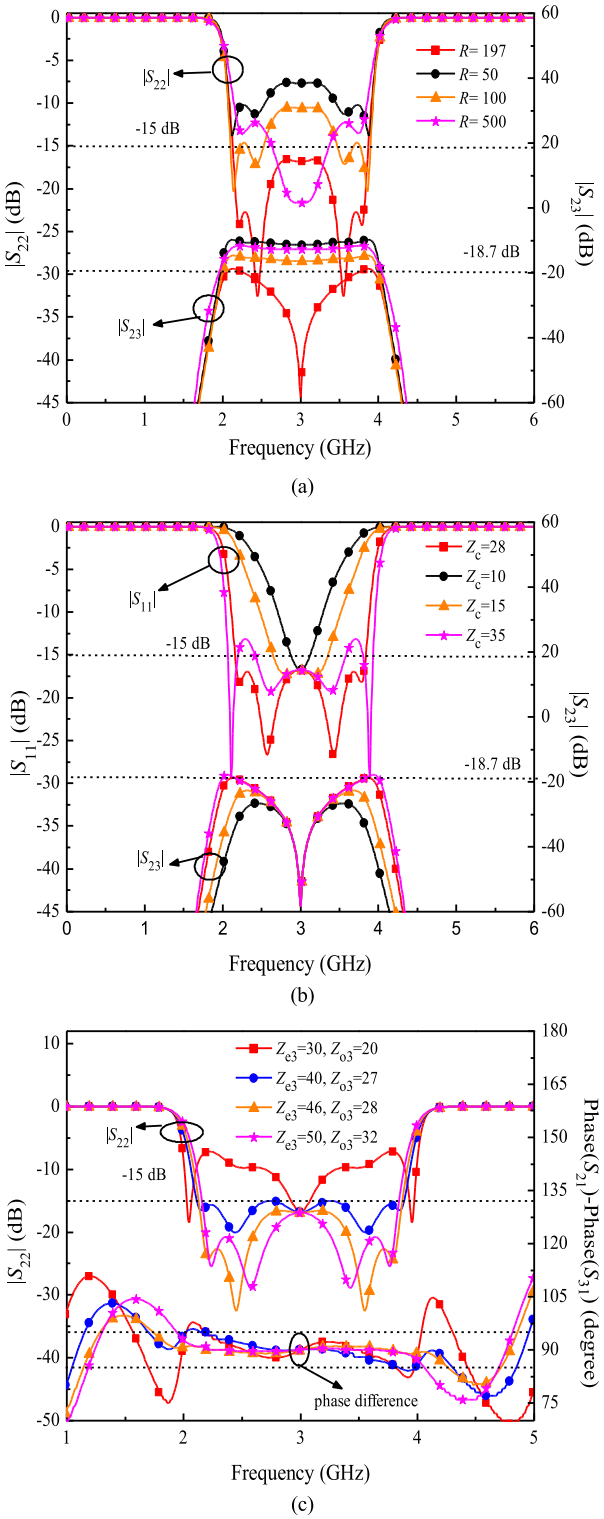

FIGURE 4. Ideal simulated *S*-parameters of the proposed wide-band filtering coupler with different values of *R*, Z_c, Z_{e3}, and Z_{o3} (Ω). (a) *R*. (b) Z_c. (c) Z_{e3} and Z_{o3}.

Combining with (10), (11) in Section II, we can get the values of Z_m and ρ are 35.94 Ω and 1.64, respectively.

Fig. 5(a) shows the changes of *S*-parameters for the proposed coupler with/without OCSs using the same optimal impedances as Fig. 4. When the proposed broadband filtering three-port coupler with OCSs, the bandwidth of 15-dB return loss is 49% ranging from 2.1 to 3.57 GHz and the all-passband isolation is below −18.6 dB. However, for the proposed coupler without OCSs, the in-band return loss is >15 dB with only 13% in the 2.8-3.2 GHz frequency band. Thus, the performance indexes involving the filtering performance, out-of-band rejection, and in-band insertion loss are significantly improved with the loaded OCSs. Additionally, the half-wavelength OCSs can expand the bandwidth and improve the skirt selectivity with no additional insertion loss by adding extra TPs at the cut-off frequency. In Fig. 5(b), the differential phase shift of 90° ± 5° has been obtained with/without OCSs. Obviously, the phase shift bandwidth of the proposed wideband filtering coupler can't be affected by the half-wavelength OCS.

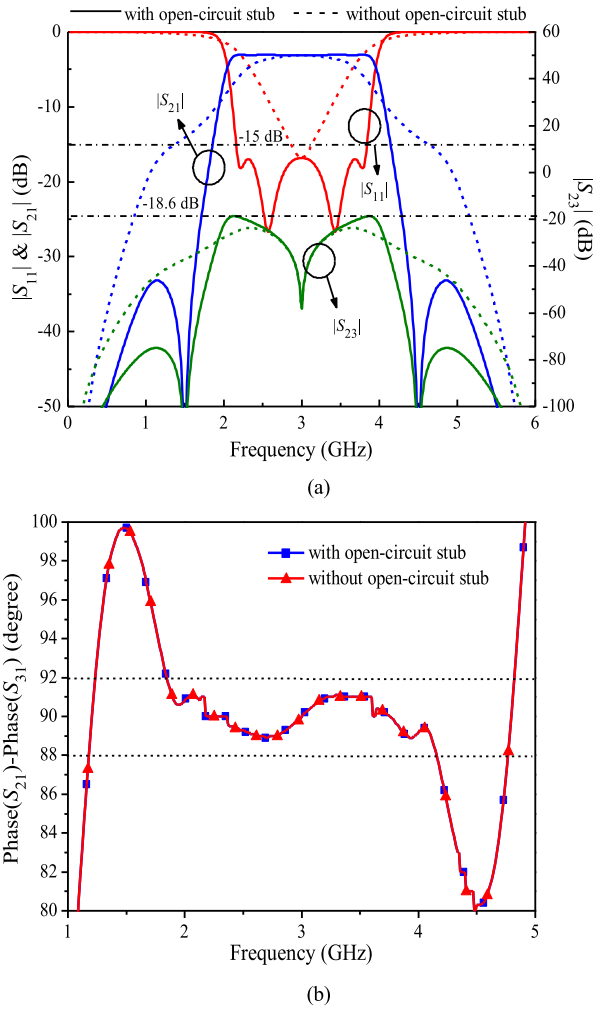

FIGURE 5. Ideal simulated *S*-parameters of the proposed wide-band filtering coupler with/without OCS. (a) S_{11}, S_{21}, and S_{23}. (b) Phase difference.

IV. CASE ANALYSIS

By using of Advanced Design System (ADS) software, three typical cases are designed and simulated to verify our proposed analytical design approaches and circuit structure.

TABLE 1. Different parameters of the three cases.

Case	Circuit parameters at 3 GHz (Ω)	FBW (%)	RL (dB)	ISO (dB)
A	Z_{e1}=153; Z_{o1}=46; Z_c=28; Z_{e2}=160; Z_{o2}=70; Z_t=50; Z_{e3}=46; Z_{o3}=28; Z_n=42; R=197; Z_S=Z_L=50; θ =π/2.	56.7 (-15 dB)	-15	-18.6
B	Z_{e1}=158; Z_{o1}=30; Z_c=60; Z_{e2}=173; Z_{o2}=65; Z_t=50; Z_{e3}=46; Z_{o3}=28; Z_n=42; R=177; Z_S=Z_L=50; θ =π/2.	71 (-15 dB)	-15	-17
C	Z_{e1}=142; Z_{o1}=22; Z_c=32; Z_{e2}=160; Z_{o2}=75; Z_t=50; Z_{e3}=42; Z_{o3}=25; Z_n=42; R=130; Z_S=Z_L=50; θ =π/2.	56.7 (-15 dB)	-20	-18

FBW: fractional bandwidth. RL: return loss. ISO, isolation.

TABLE 2. Dimensions of the fabricated cases (Unit: mm).

Parameters	W_0	W_1	W_2	W_3	W_c	W_d	W_s	S_1	L_0
Value (mm)	3.29	0.66	0.47	5.15	8.00	3.33	4.37	0.10	20.00
Parameters	S_2	S_3	L_1	L_2	L_3	L_s	L_{c1}	L_{c2}	L_{d1}
Value (mm)	0.49	0.34	16.00	16.80	13.52	14.51	14.60	14.75	44.68

All the circuit parameters and functions for three different design alternatives are listed in Table 1. Moreover, Fig. 6 illustrates the corresponding scattering parameters and phase information. It is worth noting that the lumped resistor R applied to obtain high wide-band isolation between the two output ports (ports 2 and 3).

Above all, Fig. 6(a) shows the simulated 15-dB in-band return loss bandwidth of the coupler in the proposed case A is about 56.7% from 2.15 to 3.85 GHz and the all-passband isolation is better than 18.6 dB. Furthermore, the out-of-band rejection of the coupler is less than −33.7 dB. As observed in Fig. 6(b), the bandwidth of case B is added to 71% from 1.94 to 4.07 GHz by mainly increasing the value of the characteristic impedance for the half-wavelength OCSs and slightly adjusting the value of R, whereas the all-passband isolation and the out-band rejection are declined to −17 dB and −22.86 dB, respectively. Compared with case A, the all-passband isolation is reduced to −18 dB and the stopband suppression is declined to −29.56 dB for case C. However, the in-band return loss of case C can be improved to 20 dB with a bandwidth of 45%, which is only changed by the tight degree of the input CLs. Moreover, the bandwidth of 15-dB in-band return loss is about 56.7% which is similar to case A. As illustrated in Fig. 7, it is observed that the phase difference between ports 2 and 3 of the three cases are 90° ±2° in the frequency bandwidth and these three cases achieve an excellent in-band return loss ($|S_{11}|$), and a high isolation ($|S_{23}|$). Additionally, they all showed a good filtering performance.

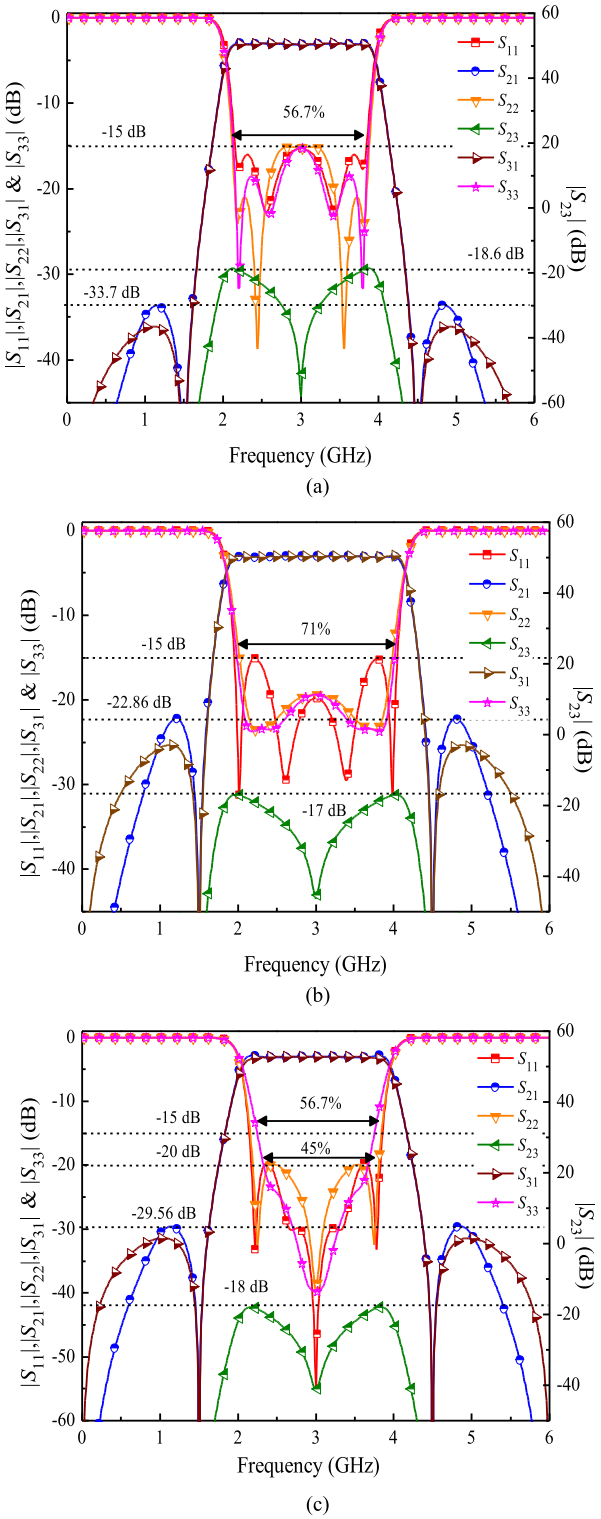

FIGURE 6. Ideal simulated *S*-parameters for typical three cases. (a) Case A. (b) Case B. (c) Case C.

V. IMPLEMENTATION AND MEASURED RESULTS

For further demonstrating the proposed theory and method, we have selected one of the cases in Section IV, i.e. case A operating at the center frequency f_0 of 3 GHz in Fig. 6(a). A Rogers RO4350B substrate featuring a dielectric constant of 3.48, a thickness of 1.524 mm, a loss tangent of 0.0037 is selected for the coupler development.

TABLE 3. Comparisons of the proposed couplers with other referenced prototypes.

Refs.	f_0 (GHz)	10-dB FBW (in-band)	Filtering/ Lower &Upper Attenuation Rates (dB/GHz)	TPs	IL/BW (stopband)	ISO (dB)	BW/ PS (±5°)	DC-Blocking
[11]	2	~70% (1.3-2.7 GHz)	No	3	N/A	-20 (1.5-2.5 GHz)	~56%	No
[12]	1.9	~89% (1.1-2.8 GHz)	No	2	N/A	-22 (1.2-2.7 GHz)	~55%	No
[24]	3	75.7% (1.92-4.19 GHz)	No	2	N/A	-15 (1-5.5 GHz)	43%	No
[25]	3	90% (1.7-4.4 GHz)	No	3	N/A	-20 (1.7-4.4 GHz)	75.67%	No
This work	3	51% (2.06-3.59 GHz)	Yes (95.35 & 82)	4	-25.7 dB (up to 1.8f_0)	-13 (all-passband)	48%	Yes (ports 2 and 3)

FBW: fractional bandwidth; RL: return loss; TPs: transmission poles; IL: insertion loss; ISO: isolation; PS: phase shift.
All the values are from the experimentally-measured results.

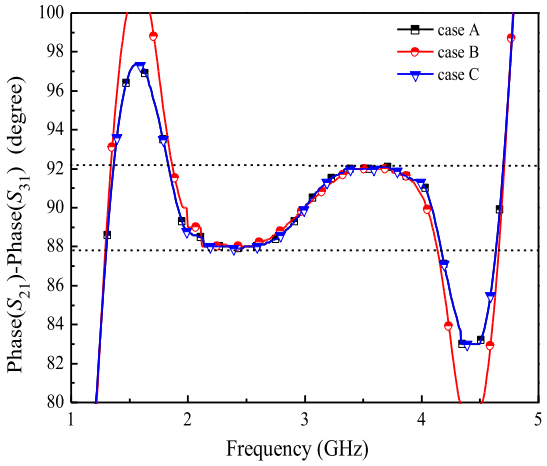

FIGURE 7. The phase difference of the ideal simulated *S*-parameters for typical three cases.

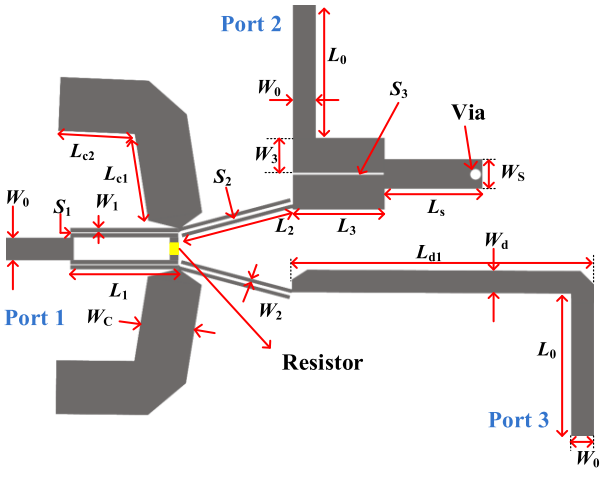

(a)

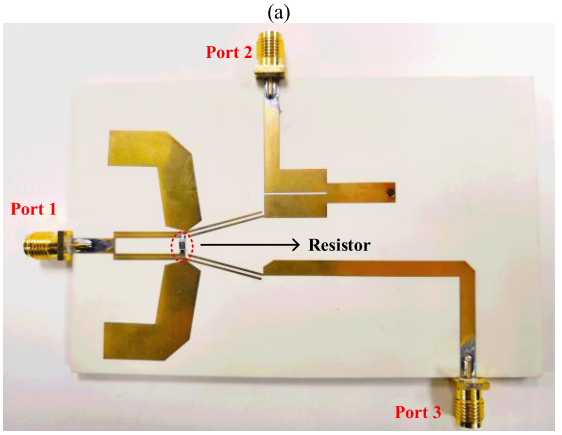

(b)

FIGURE 8. The circuit layout and photograph of the proposed wideband filtering coupler on the substrate of RO4350B. (a) Layout. (b) The photo of the fabricated prototype.

Fig. 8(a) shows the photograph of the fabricated coupler with the detailed dimensions. Note that the radius of via hole is 0.8 mm and all the dimensions are shown in Table 2. The photograph of the fabricated planar circuit board (PCB) is demonstrated in Fig. 8(b). The ideal and electromagnetic (EM) simulations are performed by ADS software, and the measured results are obtained by the vector network analyzer of ROHDE&SCHWARZ ZVA8.

Fig. 9 illustrates the EM simulations and measured results. As shown in Fig. 9(a), the bandwidth of the measured 12-dB return loss is about 49% from 2.1 to 3.57 GHz. The bandwidth for phase shifting with ±5° phase variation is from 2.1 to 3.54 GHz with a fractional bandwidth of 48% and is covered by the 12-dB return loss bandwidth. It can be seen from the measured results that both S_{21} and S_{31} have good broadband filtering performance in the passband. The magnitudes of transmission coefficients S_{21} and S_{31} coincide with each other in the bandwidth from 2.1 to 3.6 GHz. Then the measured $|S_{21}|$ and $|S_{31}|$ parameters at 3 GHz are about 3.80 and 3.89 dB, respectively. Moreover, the 25.7-dB upper stopband rejection is up to 5.4 GHz and S_{31} has a stronger

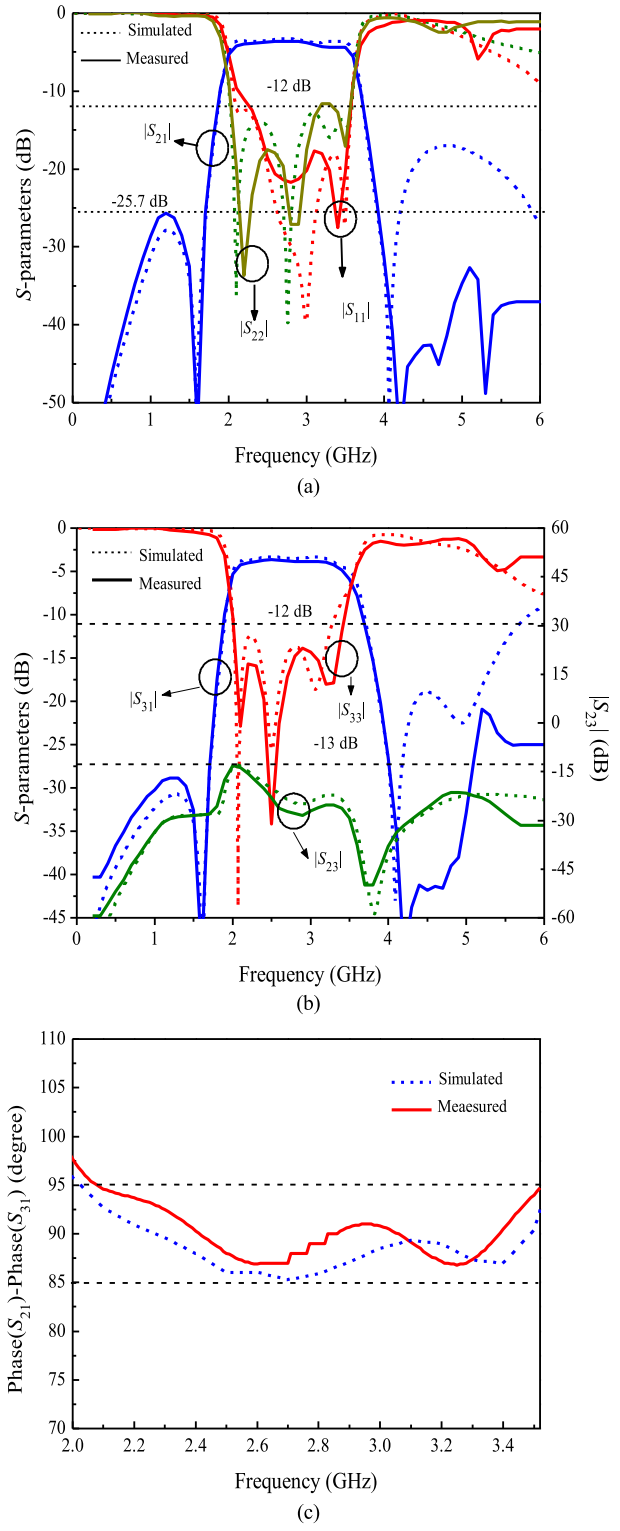

FIGURE 9. EM simulated and measured *S*-parameters of case A for (a) S_{11}, S_{21}, and S_{22}. (b) S_{21}, S_{23}, S_{31}, and S_{33}. (c) Phase difference between S_{21} and S_{31}.

stopband rejection compared with S_{21}, which can reach 28.7 dB. Besides, the measured isolation is below −13 dB across the entire passband. Moreover, the 45 dB-attenuation rate is introduced as [(45 dB-4 dB)/(f_{45dB}-f_{4dB})] to display the extreme sharp skirt selectivity. Then, the 45 dB-attenuation rate for the lower and upper side of the stopband are about 95.35 and 82, respectively.

Furthermore, the ±5° phase difference between the two output ports was observed over the operating bandwidth as shown in Fig. 9(c). Note that the maximum insertion loss of S_{21} and S_{31} is less than 3.9 dB and the magnitude difference between ports 2 and 3 is negligibly small. The simulated and measured results show that the operating bandwidth defined by the return loss depends mainly on the parameter $|S_{22}|$.

The EM simulations and measured results reveal a very good agreement. The reason for the little discrepancy between the simulated and the measured results is the junction discontinuities and the tolerance in fabrications.

In comparison with other reported work in this field, the proposed wideband filtering coupler has a wide bandwidth, good in-band return loss, high all-passband isolation and an excellent out-band suppression. The comparison data are shown in Table 3. The bandwidths of the other work are slightly higher than the designed coupler, however, by appropriately increasing the value of the half-wavelength OCSs characteristic impedance and adjusting the value of R the proposed coupler can achieve a similar bandwidth as shown in case B. In addition, compared to the previous works, the designed coupler increases filtering bandwidth and improves selectivity by increasing extra TPs. Moreover, the designed circuit has an enhanced DC-blocking function.

VI. CONCLUSION

A novel wide-band filtering three-port coupler with inherent DC-blocking function is proposed. The coupler consists of a broadband filtering power divider and a wide-band phase shifter, which features wide band and filtering performances, flat phase difference, and inherent DC-blocking function between two output ports. Three numerical cases were designed and simulated in the paper and one of the cases was actually processed. A design example with a 12-dB bandwidth of 49%, an excellent filtering performance, 25.7-dB out-of-band rejection up to 5.4 GHz, and 13-dB isolation across the entire band experimentation was verified by simulation and experimentation. Finally, a good agreement between simulation and measurement validates that the proposed coupler has a fully promising application in multi-feed CP antennas and systems for modern wireless communication.

REFERENCES

[1] Q. Liu, J. Shen, J. Yin, H. Liu, and Y. Liu, "Compact 0.92/2.45-GHz dual-band directional circularly polarized microstrip antenna for handheld RFID reader applications," *IEEE Trans. Antennas Propag.*, vol. 63, no. 9, pp. 3849–3856, Sep. 2015.

[2] Q. Liu, J. Shen, H. Liu, and Y. Liu, "Dual-band circularly-polarized unidirectional patch antenna for RFID reader applications," *IEEE Trans. Antennas Propag.*, vol. 62, no. 12, pp. 6428–6434, Dec. 2014.

[3] K. L. Chung, "High-performance circularly polarized antenna array using metamaterial-line based feed network," *IEEE Trans. Antennas Propag.*, vol. 61, no. 12, pp. 6233–6237, Dec. 2013.

[4] F. Lin and H. Ma, "Design of a class of filtering couplers with reconfigurable frequency," *IEEE Trans. Microw. Theory Techn.*, vol. 66, no. 9, pp. 4017–4028, Sep. 2018.

[5] R. Gómez-García, M.-Á. Sánchez-Soriano, M. Sánchez-Renedo, G. Torregrosa-Penalva, and E. Bronchalo, "Low-pass and bandpass filters with ultra-broad stopband bandwidth based on directional couplers," *IEEE Trans. Microw. Theory Techn.*, vol. 61, no. 12, pp. 4365–4375, Dec. 2013.

[6] J. Shi *et al.*, "A balanced filtering branch-line coupler," *IEEE Microw. Wireless Compon. Lett.*, vol. 26, no. 2, pp. 119–121, Feb. 2016.

[7] Q. Shao, F.-C. Chen, Q.-X. Chu, and M. J. Lancaster, "Novel filtering 180° hybrid coupler and its application to 2×4 filtering butler matrix," *IEEE Trans. Microw. Theory Techn.*, vol. 66, no. 7, pp. 3288–3296, Jul. 2018.

[8] J. Reed and G. J. Wheeler, "A method of analysis of symmetrical four-port networks," *IRE Trans. Microw. Theory Techn.*, vol. 4, no. 4, pp. 246–252, Oct. 1956.

[9] R. Levy and L. F. Lind, "Synthesis of symmetrical branch-guide directional couplers," *IEEE Trans. Microw. Theory Techn.*, vol. MTT-16, no. 2, pp. 80–89, Feb. 1968.

[10] C.-W. Tang, M.-G. Chen, Y.-S. Lin, and J.-W. Wu, "Broadband microstrip branch-line coupler Broadband microstrip branch-line coupler," *Electron. Lett.*, vol. 42, no. 25, pp. 1458–1460, Dec. 2006.

[11] Y.-H. Chun and J.-S. Hong, "Compact wide-band branch-line hybrids," *IEEE Trans. Microw. Theory Techn.*, vol. 54, no. 2, pp. 704–709, Feb. 2006.

[12] H.-J. Yoon and B.-W. Min, "Two section wideband 90° hybrid coupler using parallel-coupled three-line," *IEEE Microw. Wireless Compon. Lett.*, vol. 27, no. 6, pp. 548–550, Jun. 2017.

[13] A. M. Abbosh and M. E. Bialkowski, "Design of compact directional couplers for uwb applications," *IEEE Trans. Microw. Theory Techn.*, vol. 55, no. 2, pp. 189–194, Feb. 2007.

[14] D. N. A. Zaidel, S. K. A. Rahim, N. Seman, C. L. Chew, and N. H. Khamis, "A design of octagon-shaped 3-dB ultra wideband coupler using multilayer technology," *Microw. Opt. Technol. Lett.*, vol. 55, no. 1, pp. 127–130, Jan. 2013.

[15] Y. Wu, W. Sun, S. W. Leung, Y. Diao, K. H. Chan, and Y. M. Siu, "Single-layer microstrip high-directivity coupled-line coupler with tight coupling," *IEEE Trans. Microw. Theory Techn.*, vol. 61, no. 2, pp. 746–753, Feb. 2013.

[16] Y. Wu, J.-Y. Shen, Y. Liu, S.-W. Leung, and Q. Xue, "Miniaturized arbitrary phase-difference couplers for arbitrary coupling coefficients," *IEEE Trans. Microw. Theory Techn.*, vol. 61, no. 6, pp. 2317–2324, Jun. 2013.

[17] M. A. Maktoomi, M. S. Hashmi, and F. M. Ghannouchi, "Theory and design of a novel wideband DC isolated Wilkinson power divider," *IEEE Microw. Wireless Compon. Lett.*, vol. 26, no. 8, pp. 586–588, Aug. 2016.

[18] S. S. Gao, S. Sun, and S. Xiao, "A novel wideband bandpass power divider with harmonic-suppressed ring resonator," *IEEE Microw. Wireless Compon. Lett.*, vol. 23, no. 3, pp. 119–121, Mar. 2013.

[19] D. Chen, L. Zhu, and C. Cheng, "Dual-resonant-mode (DRM) impedance transformer and its application to wideband 3 dB power divider," *IEEE Microw. Wireless Compon. Lett.*, vol. 23, no. 9, pp. 471–473, Sep. 2013.

[20] X. Wang, J. Wang, G. Zhang, J.-S. Hong, and W. Wu, "Dual-wideband filtering power divider with good isolation and high selectivity," *IEEE Microw. Wireless Compon. Lett.*, vol. 27, no. 12, pp. 1071–1073, Dec. 2017.

[21] L. Jiao, Y. Wu, Y. Liu, Q. Xue, and Z. Ghassemlooy, "Wideband filtering power divider with embedded transversal signal-interference sections," *IEEE Microw. Wireless Compon. Lett.*, vol. 27, no. 12, pp. 1068–1070, Dec. 2017.

[22] C.-W. Tang and J.-T. Chen, "A design of 3-dB wideband microstrip power divider with an ultra-wide isolated frequency band," *IEEE Trans. Microw. Theory Techn.*, vol. 64, no. 6, pp. 1806–1811, Jun. 2016.

[23] Z.-Y. Zhang, Y.-X. Guo, L. C. Ong, and M. Y. W. Chia, "A new wide-band planar balun on a single-layer PCB," *IEEE Microw. Wireless Compon. Lett.*, vol. 15, no. 6, pp. 416–418, Jun. 2005.

[24] Y. Wu, Q. Liu, J. Shen, and Y. Liu, "A novel wide-band hybrid coupler using coupled-line power divider and improved coupled-line phase shifter," *J. Electromagn. Waves Appl.*, vol. 27, no. 3, pp. 374–384, Nov. 2013.

[25] R.-C. Han, R.-Y. Sun, and S.-H. Shi, "A wideband planar hybrid coupler using coupled-line power divider and broadband phase shifter," in *Proc. 6th Asia–Pacific Conf. Antennas Propag. (APCAP)*, Oct. 2017, pp. 1–3.

[26] Z. Zhuang, Y. Wu, Y. Liu, and Z. Ghassemlooy, "Wideband bandpass-to-all-stop reconfigurable filtering power divider with bandwidth control and all-passband isolation," *IET Microw. Antennas Propag.*, vol. 12, no. 11, pp. 1852–1858, Sep. 2018.

[27] Q. Liu, H. Liu, and Y. Liu, "Compact ultra-wideband 90° phase shifter using short-circuited stub and weak coupled line," *Electron. Lett.*, vol. 50, no. 20, pp. 1454–1456, Sep. 2014.

WEIMIN WANG received the B.S. degree in communication engineering, the M.S. degree in electromagnetic field and microwave technology, and the Ph.D. degree in electronic science and technology from the Beijing University of Posts and Telecommunications (BUPT), Beijing, China, in 1999, 2004, and 2014, respectively. In 2014, she joined BUPT, where she is currently an Associate Professor with the School of Electronic Engineering. Her research interests include electromagnetic field, antennas, and MIMO OTA measurement.

YANA ZHENG received the B.S. degree in electronic information science and technology from Shanxi University, Shanxi, China, in 2018. She is currently pursuing the M.S. degree with the Beijing University of Posts and Telecommunications, Beijing, China. Her research interests include microwave components and antennas.

YONGLE WU (M'12–SM'15) received the B.Eng. degree in communication engineering and the Ph.D. degree in electronic engineering from the Beijing University of Posts and Telecommunications (BUPT), Beijing, China, in 2006 and 2011, respectively. In 2010, he was a Research Assistant with the City University of Hong Kong, Hong Kong.

In 2011, he joined BUPT, where he is currently a Full Professor with the School of Electronic Engineering. His research interests include microwave components, circuits, antennas, and wireless system design.

ZHENG ZHUANG received the B.S. degree in electronic science and technology from the Beijing University of Chemical Technology, Beijing, China, in 2015. He is currently pursuing the Ph.D. degree with the Beijing University of Posts and Telecommunications (BUPT). In 2015, he started his research as a graduate at BUPT. His research interests include microwave passive components, power amplifiers, and transformation optics.

YUANAN LIU received the B.E., M.Eng., and Ph.D. degrees in electrical engineering from the University of Electronic Science and Technology of China, Chengdu, China, in 1984, 1989, and 1992, respectively.

In 1984, he joined the 26th Institute of Electronic Ministry of China to develop the inertia navigating system. In 1992, he began his first postdoctoral position at the EMC Laboratory, Beijing University of Posts and Telecommunications (BUPT), Beijing, China. In 1995, he started his second postdoctoral position at the Broadband Mobile Laboratory, Department of System and Computer Engineering, Carleton University, Ottawa, ON, Canada. Since 1997, he has been a Professor with the Wireless Communication Center, College of Telecommunication Engineering, BUPT, where he is involved in the development of next-generation cellular systems, wireless LAN, Bluetooth application for data transmission, EMC design strategies for high-speed digital systems, and EMI and EMS measuring sites with low cost and high performance.